Gangliosides interact with synaptotagmin to form the high-affinity receptor complex for botulinum neurotoxin B

Alessandra Flores[a,b,1], Jorge Ramirez-Franco[a,b,1], Richard Desplantes[a,b], Kévin Debreux[a,b], Géraldine Ferracci[b,c], Florian Wernert[a,b], Marie-Pierre Blanchard[b,c], Yves Maulet[a,b], Fahamoe Youssouf[a,b], Marion Sangiardi[a,b], Cécile Iborra[a,b], Michel Robert Popoff[d], Michael Seagar[a,b], Jacques Fantini[a,b], Christian Lévêque[a,b], and Oussama El Far[a,b,2]

[a]Unité de Neurobiologie des Canaux Ioniques et de la Synapse, INSERM UMR_S 1072, 13015 Marseille, France; [b]Aix-Marseille Université, 13015 Marseille, France; [c]Institut de Neurophysiopathologie, CNRS UMR 7051, 13015 Marseille, France; and [d]Bacterial Toxins, Équipe de Recherche Labellisée 6002, Institut Pasteur, 75015 Paris, France

Edited by Solomon H. Snyder, Johns Hopkins University School of Medicine, Baltimore, MD, and approved August 1, 2019 (received for review May 15, 2019)

Botulinum neurotoxin type B (BoNT/B) recognizes nerve terminals by binding to 2 receptor components: a polysialoganglioside, predominantly GT1b, and synaptotagmin 1/2. It is widely thought that BoNT/B initially binds to GT1b then diffuses in the plane of the membrane to interact with synaptotagmin. We have addressed the hypothesis that a GT1b–synaptotagmin *cis* complex forms the BoNT/B receptor. We identified a consensus glycosphingolipid-binding motif in the extracellular juxtamembrane domain of synaptotagmins 1/2 and confirmed by Langmuir monolayer, surface plasmon resonance, and circular dichroism that GT1b interacts with synaptotagmin peptides containing this sequence, inducing α-helical structure. Molecular modeling and tryptophan fluorescence spectroscopy were consistent with the intertwining of GT1b and synaptotagmin, involving *cis* interactions between the oligosaccharide and ceramide moieties of GT1b and the juxtamembrane and transmembrane domains of synaptotagmin, respectively. Furthermore, a point mutation on synaptotagmin, located outside of the BoNT/B-binding segment, inhibited GT1b binding and blocked GT1b-induced potentiation of BoNT/B binding to synaptotagmin-expressing cells. Our findings are consistent with a model in which a preassembled GT1b–synaptotagmin complex constitutes the high-affinity BoNT/B receptor.

botulinum neurotoxin B receptor | synaptotagmin | gangliosides

Botulinum neurotoxins (BoNTs) reach their neuronal targets through several steps. After oral ingestion, they bind to epithelial cells of the digestive tract then escape from the gastrointestinal milieu, mainly by trancytosis and barrier disruption, into the circulation (1, 2). BoNTs then cross the endothelial barrier and attain peripheral nerve terminals, binding with high affinity to specific neuronal receptors. BoNT serotypes A, B, and E (BoNT/A, BoNT/B, and BoNT/E), the main agents of human botulism, target mainly neuromuscular junctions (NMJ), where they impair acetylcholine release and consequently cause flaccid paralysis (3).

At the molecular level, BoNTs are AB toxins composed of 2 polypeptides, the heavy (100 kDa) and the light (50 kDa) chains, linked by a disulphide bridge and noncovalent interactions (1, 4). All BoNT serotypes employ a similar mechanism of intoxication. The carboxy and amino-terminal domains of the heavy chain confer respectively receptor-binding and light chain translocation through the endocytic vesicle membrane into the cytosol. The light chain is a zinc-dependent endopeptidase responsible for the inactivation of SNARE proteins essential for neurotransmitter release. BoNT/B cleaves synaptobrevin (VAMP), which is an integral protein of the synaptic vesicle membrane, whereas BoNT/A and BoNT/E cleave SNAP-25 (synaptosomal-associated protein of 25 kDa), a protein located on the cytosolic face of the presynaptic membrane (1–3).

BoNT/A, B, and E receptors are composed of plasma membrane gangliosides and intraluminal domains of transmembrane synaptic vesicle proteins that become accessible at the presynaptic membrane upon exocytosis. BoNT/A and E bind to the synaptic vesicle protein 2 (SV2), while BoNT/B binds synaptotagmin (SYT isoforms 1 and 2).

Gangliosides are amphiphilic glycosphingolipid molecules predominantly anchored, via their ceramide group, in the outer leaflet of plasma membranes. Their extracellular polar part is composed of several characteristic sugar molecules with the negatively charged sialic acids at precise positions. Gangliosides are major components of neuronal membranes accounting for 10 to 20% of total membrane lipids of the outer leaflet and act as cell-surface receptors for certain viruses, bacteria, microbial toxins, and antibodies (5, 6). GM1, GD1a, GD1b, and GT1b account for >90% of adult mammalian brain gangliosides. They differ in the number and position of their sialic acids linked to a common tetrasaccharide core (7, 8), with GT1b being the preferred form recognized by BoNT/B (9). Because of their high content in long saturated alkyl chains and their propensity to associate with other sphingolipids and cholesterol, gangliosides are thought to promote the formation of tightly packed lipid domains that are in a dynamic equilibrium with the less-ordered

Significance

Botulism is induced by *Clostridium* botulinum neurotoxins (BoNTs). At neuromuscular junctions, BoNT/B binds to dual receptors: a plasma membrane resident polysialoganglioside and synaptotagmin, a synaptic vesicle protein transiently inserted in neuronal membranes upon exocytosis. It is widely thought that BoNT binds initially to gangliosides and that this binary complex then diffuses to interact with synaptotagmin. Here, we show that the true BoNT/B receptor is the preassembled GT1b–SYT complex and that the α-helical structure of the BoNT/B binding domain of synaptotagmin found in previous structural studies is induced by the ganglioside before it ever meets the toxin. BoNT/B thus exploits a preexisting protein–glycolipid complex of yet unknown physiological function.

Author contributions: M. Seagar, C.L., and O.E.F. designed research; A.F., J.R.-F., R.D., K.D., G.F., F.W., M.-P.B., Y.M., F.Y., M. Sangiardi, C.I., J.F., and C.L. performed research; M.R.P. contributed new reagents/analytic tools; M. Seagar, C.L., and O.E.F. analyzed data; and M. Seagar, J.F., C.L., and O.E.F. wrote the paper.

The authors declare no conflict of interest.

This article is a PNAS Direct Submission.

[1]A.F. and J.R.-F. contributed equally to this work.

[2]To whom correspondence may be addressed. Email: oussama.el-far@inserm.fr.

This article contains supporting information online at www.pnas.org/lookup/suppl/doi:10.1073/pnas.1908051116/-/DCSupplemental.

Published online August 20, 2019.

environment (10). Moreover, the hydrogen-bonding ability of their headgroups results in extensive ganglioside and protein–ganglioside interactions in *cis* or *trans* configuration (8, 11). In neurons, gangliosides are involved in a diverse range of functions including synaptic transmission (8) and colocalize with proteins having a major role in neurotransmission such as SNARE proteins (11, 12).

SYT 1 and 2 are expressed in synaptic vesicles and play an essential function in neurotransmitter release, acting as the primary calcium sensors that trigger exocytosis. SYT also plays a major role in clathrin-dependent endocytosis in the periactive zone (13). They consist of a small luminal N-terminal segment that harbors *N*- and *O*-glycosylation sites (14), a single transmembrane (TM) domain, and a large cytoplasmic calcium, phospholipid, and SNARE complex binding domain participating in membrane bilayer deformation necessary for SV fusion (15). Upon exocytosis the N-terminal domain of SYT becomes accessible at the cell surface. Although there are minor sequence differences between SYT1 and SYT2 N-terminal domains, the affinity of BoNT/B for rat SYT2 is more than 2 orders of magnitude higher than for rat SYT1 (16). Interestingly, however, a single amino acid difference between rat and human SYT2 drastically diminishes BoNT/B binding affinity for the latter and consequently SYT1 is considered to be the major receptor for BoNT/B in humans at NMJ (17) and autonomic nerve terminals (18).

X-ray crystallography has shown that the trefoil C-terminal domain of BoNT/B carries 2 vicinal but independent binding pockets. One pocket accommodates the polar part of a ganglioside, while the other interacts mainly with hydrophobic amino acids in the extracellular juxtamembrane domain of SYT (18, 19). Although this SYT domain is unstructured in solution it has an α-helical structure in the toxin binding pocket (9, 16, 19). Structural modeling data and substitution of several amino acids between SYT1 and SYT2 have suggested a conserved BoNT/B binding mode for both SYT isoforms (16, 18).

Although structural, biochemical, and functional studies support the idea that a double receptor anchorage of BoNT/B is responsible for the exquisite neurotropic specificity of BoNT/B, the precise sequence of events that lead to BoNT/B binding is unknown. The current "dual receptor" hypothesis proposes that circulating BoNTs are initially captured by gangliosides and thus concentrated at the presynaptic surface. The GT1b–BoNT complex would then migrate in the plane of the membrane, facilitating subsequent binding to the protein receptor, making the interaction almost irreversible and allowing receptor-mediated endocytosis (10, 20). However, it was proposed that the toxin simultaneously binds both receptors located in very close proximity (21). This alternative view is moreover supported by the very low binding affinity of BoNT to gangliosides compared to SYT (22). Recently a new partner has been implicated in the mechanisms that orchestrate BoNT/B binding to neurons, as membrane lipids have recently been shown to interact with a hydrophobic loop of BoNT/B located between the SYT and the GT1b binding pockets (22).

In this paper we reexamined the interaction between BoNT/B and its coreceptors. Using a range of molecular approaches, we first identified a consensus glycosphingolipid-binding motif in SYT and then characterized a direct interaction between its juxtamembrane extracellular domain and the polar moiety of GT1b. Our results indicate that this interaction extends into the membrane, involving the TM region of SYT and the ceramide moiety, corroborating the view that the SYT–GT1b complex forms a highly stable structure, constituting a preassembled high-affinity BoNT/B receptor. Our data suggest that GT1b binding confers α-helical structure to the extracellular juxtamembrane domain of SYT which is then accommodated in the SYT binding pocket of BoNT/B, while subsequent occupancy of the ganglioside binding pocket would then stabilize BoNT/B binding.

Results

Assessment of BoNT/B Binding to SYT2 or GT1b in a Cellular Context. The current model for BoNT/B intoxication proposes that BoNT/B first attaches to the membrane by binding to gangliosides and then moves laterally to bind SYT. We revisited this question by investigating BoNT/B binding to SYT2 or GT1b separately. These experiments were performed in SYT1- and SYT2-deficient PC12 cells transfected with SYT2 (PC12ΔSYT1 *SYT2*$^{+}$) and treated with PPMP (DL-*threo*-1-phenyl-2-palmitoylamino-3-morpholino-1-propanol), an inhibitor of GT1b synthesis that abolishes most of its expression (98 ± 2%, $n = 3$ independent experiments; *SI Appendix*, Fig. S1 *A* and *B*). BoNT/B binding to PC12 cells was not detectable either with endogenous or exogenously added GT1b, in the absence of SYT (*SI Appendix*, Fig. S1*A*).

Moderate but specific BoNT/B binding was detected on PC12 cells expressing SYT2 and treated with PPMP. Staining was mainly detected at the cell surface, colocalized with SYT2 and delineated transfected cells (Fig. 1*A*), whereas no signal was observed on cells transfected with carrier vector expressing enhanced green fluorescent protein (EGFP) (lower lane). In the presence of PPMP and upon increasing BoNT/B concentration from 5 to 40 nM, BoNT/B binding was enhanced by a factor of 3 (Fig. 1 *A* and B). The binding affinity of BoNT/B for SYT2 in the absence of GT1b was measured using SYT2-expressing exosomes that do not contain GT1b or GD1a (23) and yielded a dissociation constant (K_d) of 40 nM (Table 1 and *SI Appendix*, Fig. S1*C*). As a negative binding control, BoNT/E, which binds SV2, did not show any interaction in this paradigm (*SI Appendix*, Fig. S1*C*). These results indicate that while BoNT/B binds specifically to SYT2 in the absence of GT1b, binding to GT1b alone was not detectable.

In order to study on living cell membranes the potential proximity of SYT2 and GT1b coreceptors, close enough to capture BoNT/B, we used SYT2-transfected PC12 cells maintained on ice to reduce membrane dynamics and receptor diffusion. We quantified BoNT/B binding using a sensitive cell-based colorimetric assay in the absence or presence of PPMP. Under these conditions, BoNT/B specifically bound to SYT2-transfected cells (Fig. 1*C*). This binding was totally abolished upon preincubation of BoNT/B with a neutralizing antibody used to block BoNT/B intoxication (23). Interestingly, pretreatment with PPMP decreased BoNT/B binding by 64 ± 3% ($n = 3$ independent experiments) (Fig. 1*D*). These results indicate that GT1b can still potentiate BoNT/B binding under limited membrane diffusion and suggest that there is a pool of SYT2 and GT1b coreceptors in sufficient proximity to allow toxin binding in the absence of lateral diffusion in the plane of the membrane.

Quantification of the Effect of GT1b on BoNT/B Binding to SYT2. We compared the affinity and the kinetic binding constants of the interaction between BoNT/B and SYT2 expressed in exosomes, in the presence and absence of GT1b, using surface plasmon resonance spectroscopy (SPR). Insertion of exogenous GT1b in exosomal membranes induced an 80-fold increase in affinity ($K_d = 0.5$ nM; Table 1 and ref. 23) compared to the condition in the absence of GT1b (40 nM). This increment is driven by a 20-fold increase in k_{on} (1.5 ± 0.2 vs. 31 ± 12 × 10^4 $M^{-1}{\cdot}s^{-1}$) and a 4-fold decrease in k_{off} (5.6 ± 0.1 vs. 1.5 ± 0.6 × 10^{-4} s^{-1} [Table 1]). An estimation of the contribution of electrostatic interactions was carried out by increasing salt concentration in the running buffer. As shown in Table 1, moderate salt concentration increase (350 mM NaCl) induced a dramatic decrease in the association kinetic constant of BoNT/B with SYT2/GT1b, whereas it hardly influenced the k_{on} on SYT2. Under these conditions, a similar on-rate (k_{on}) was observed for BoNT/B binding to both SYT2/GT1b (0.8 ± 0.2 × 10^4 $M^{-1}{\cdot}s^{-1}$) and SYT2 (0.8 ± 0.1 × 10^4 $M^{-1}{\cdot}s^{-1}$), thus losing the potentiation by GT1b. In contrast, the increment in

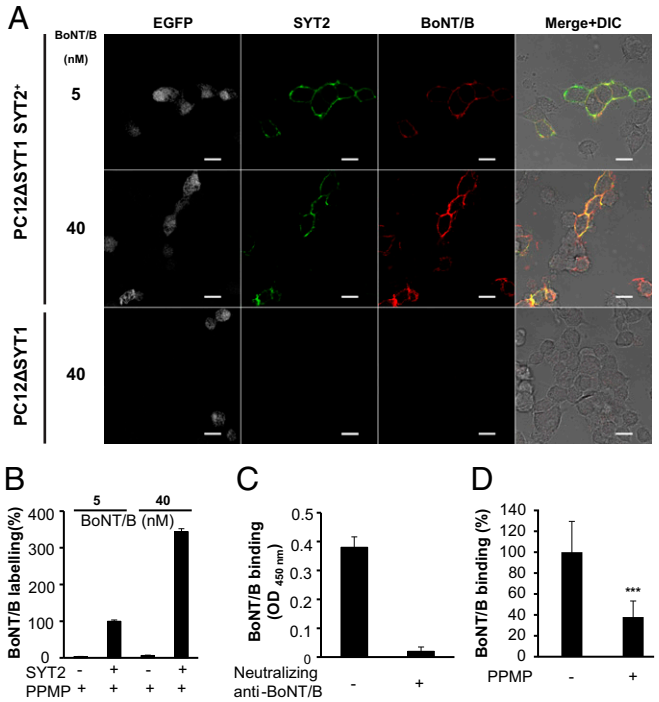

Fig. 1. BoNT/B binding to PC12 cells transfected with SYT2. (*A*) Immunofluorescence staining of SYT2 expressed in PC12 cells. PC12ΔSYT1 cells expressing or not expressing SYT2 were treated with PPMP and incubated 45 min with 5 or 40 nM BoNT/B in the presence of 1 μg/mL of mAb anti-SYT2 (8G2b) directed against its N-terminal extremity. Anti-BoNT/B staining results in a specific labeling at the plasma membrane colocalizing with SYT2. The right column shows merge signals associated with phase contrast captures. (Scale bars, 15 μm.) The lower lane corresponds to cells transfected with the carrier vector pIRES-EGFP. (*B*) Relative quantification of BoNT/B binding at 5 and 40 nM to SYT2 expressing PC12ΔSYT1 treated with PPMP. Immunofluorescence signals were measured from the experiment in *A*, taking the labeling at 5 nM as 100% (2 independent experiments with 60 cells and 79 cells for BoNT/B at 5 and 40 nM, respectively). Data were normalized to SYT2 staining with 8G2b. (*C*) ELISA-based determination of BoNT/B binding to PC12 cells expressing SYT2 at 4 °C. PC12ΔSYT1 cells transfected with SYT2 containing endogenous levels of GT1b were incubated 45 min on ice with BoNT/B (5 nM) in the presence or absence of neutralizing anti-BoNT/B antibody. BoNT/B binding was revealed using anti-BoNT/B and the nonspecific signal on PC12 cells transfected with the carrier vector pIRES-EGFP was subtracted. Results are representative of 2 independent experiments with assays in triplicate. (*D*) Effect of PPMP on BoNT/B binding to SYT2-transfected PC12 cells at 4 °C. Cell ELISA was performed as in *C* with cells treated or not with PPMP. Nonspecific binding to PC12 cells transfected with carrier vector was subtracted. Data are from 3 independent experiments performed in triplicate. All data are means ± SD and Mann–Whitney *U* test 1-tailed statistical analysis was performed. ***$P = 0.0004$.

ionic strength slightly increased the dissociation rate (k_{off}) of BoNT/B from both SYT2 (5.6 to 18.4 × 10^{-4} s^{-1}) and SYT2/GT1b (1.5 to 3.1 × 10^{-4} s^{-1}) exosomes (Table 1). Taken together these results suggest that GT1b strongly increases BoNT/B affinity for SYT2, mainly via electrostatic interactions. Moreover, BoNT/B binding to SYT2 alone, as well as to SYT2/GT1b, can be fitted using a simple homogenous 1:1 model (*SI Appendix*, Fig. S1*C* and ref. 23), consistent with a single receptor site as if SYT and GT1b were closely positioned or already preassembled.

The Juxtamembrane Domains of SYT1 and SYT2 Contain a Conserved Glycosphingolipid-Binding Sequence and Directly Interact with GT1b. A careful examination of the complete N-terminal sequences of SYT revealed that SYT1 and SYT2 share a consensus glycosphingolipid-binding motif (24, 25) in their membrane proximal region, illustrated in gray in Fig. 2*A*. This typical sequence K/R/H(X1-4)-F/Y-(X4-5)-K/R/H is composed of a central hydrophobic amino acid flanked by basic amino acids or histidine at defined positions and mostly overlaps with the BoNT/B binding site (F_{39}-L_{50} for SYT1 and F_{47}-I_{58} for SYT2) that was formerly determined by structural analysis (9). To assess whether this motif is a functional glycosphingolipid-binding domain, we used the Langmuir monolayer method and investigated the binding, to various gangliosides, of synthetic SYT1 (pSYT1 41-52) and SYT2 (pSYT2 49-60) peptides (*SI Appendix*, Fig. S2), corresponding respectively to the predicted juxtamembrane glycosphingolipid-binding domain of SYT1 and 2. Both wild-type (WT) peptides, but not the scrambled sequences (pSYT scr) (*SI Appendix*, Fig. S2), interacted with GT1b (Fig. 2*B*). The peptides bound GT1b better than other gangliosides (Fig. 2 *C* and *D*) such as GM1 and GM3 and did not bind the sphingolipid lyso-lactosylceramide. The specificity of the binding was confirmed by SPR using single bilayer liposomes, immobilized on a hydrophobic sensor chip. For these experiments, longer SYT peptides (pSYT1 32-57 and pSYT2 40-66), as well as peptides containing amino acid substitutions (pSYT1 32-57 K_{43}A, F_{46}A, K_{52}A, pSYT2 40-66 F_{54}A, and F_{55}A) that disrupt the consensus site, were synthesized (*SI Appendix*, Fig. S2). pSYT1 and pSYT2, but not mutated peptides, interacted with GT1b in liposomes (Fig. 2 *E* and *F*). Affinity constants from equilibrium analysis of peptide interactions with the GT1b-containing liposomes were determined, yielding K_ds of 3.1 ± 0.2 and 3.3 ± 0.7 μM for pSYT1 and pSYT2, respectively ($n = 4$ independent experiments). No binding occurred to phosphatidylserine- or phosphatidylglycerol-based liposomes that have negative charges similar to GT1b-containing liposomes (Fig. 2 *E* and *F*), indicating that recognition of GT1b by pSYT involves more than a simple electrostatic attraction via the 3 negative charges of GT1b sialic acid groups.

GT1b Promotes the Formation of an α-Helix in SYT. We performed circular dichroism (CD) spectroscopy to determine whether GT1b binding drives conformational changes in SYT. The SYT1 and SYT2 peptides (pSYT1 41-52 and pSYT2 49-60), encompassing the sphingolipid-binding domain displayed random structure in solution (Fig. 3 *A* and *B*, dashed line). In the presence of GT1b, WT peptides exhibited 2 characteristic minima at 208 and 222 nm typical of an α-helix, while no conformational change was noticeable with scrambled peptides (*SI Appendix*,

Table 1. Affinity of BoNT/B for SYT2 and SYT2/GT1b exosomes

Toxin	Receptor	NaCl, mM	k_{on} (×10^4 M^{-1}·s^{-1})	k_{off} (×10^{-4} s^{-1})	K_d (×10^{-9} M)	*n*
BoNT/B	SYT2	150	1.5 ± 0.2	5.6 ± 0.1	40.3 ± 0.5	6
		350	0.8 ± 0.1	18.4 ± 3.0	228.0 ± 31.9	4
	SYT2 + GT1b	150	31.0 ± 12	1.5 ± 0.6	0.5 ± 0.05	3
		350	0.8 ± 0.2	3.1 ± 0.9	52.5 ± 19.6	6

K_ds were determined with a 1:1 Langmuir model, as described in *Experimental Procedures* using buffer containing physiological (150 mM) or higher NaCl (350 mM) concentrations. *n* represents independent experiments in 150 mM NaCl conditions and multiple determinations from 2 independent experiments in 350 mM NaCl condition. Values are means ± SEM.

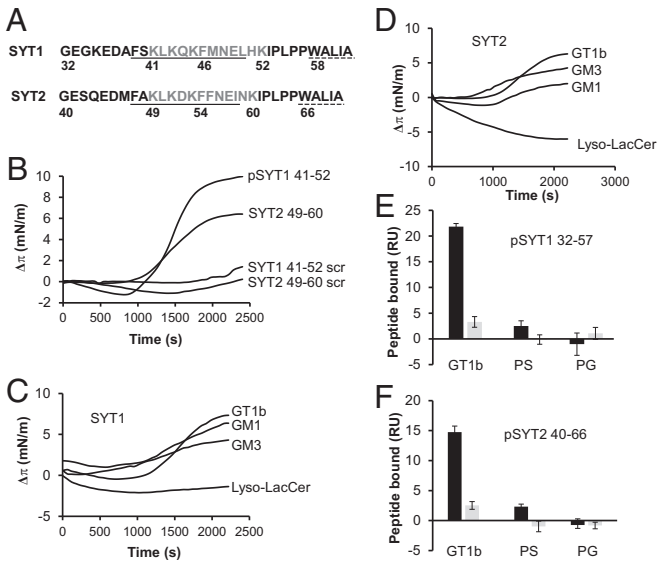

Fig. 2. SYT interaction with gangliosides. (*A*) Glycosphingolipid-binding motif in the juxtamembrane extracellular domain of rat SYT1 and SYT2. The ganglioside binding motifs of SYT1 and SYT2 are indicated by gray letters according to the following consensus (K/R/H (X1-4) – F/Y-(X4-5)- K/R/H). The beginning of the TM domain is underlined with dotted lines. The continuous line indicates the BoNT/B binding domain. (*B*) Interaction of the juxtamembrane extracellular domain of SYT1 and SYT2 with a GT1b monolayer. The data show the real-time changes of surface pressure following injection of 1 μM of pSYT1 41-52, pSYT2 49-60 peptides or corresponding scrambled peptides (pSYT1 41-52 scr. and pSYT2 49-60 scr.) beneath GT1b monolayer, prepared at an initial surface pressure of 15 to 17 $mN{\cdot}m^{-1}$. Each curve is representative of 3 separate experiments (SD < 15%). (*C* and *D*) Ganglioside binding specificity of the juxtamembrane extracellular domain of SYT1 and SYT2. Real-time representation of surface pressure changes following injection of 1 μM of pSYT1 41-52 and pSYT2 49-60 peptides with monolayers of Lys-LacCer, GM1, GM3, and GT1b (initial surface pressure of 15 to 17 $mN{\cdot}m^{-1}$). Each curve is representative of 3 separate experiments (SD < 15%). (*E*) Specificity of SYT1 interaction with GT1b inserted in bilayer vesicles. DMPC liposomes containing GT1b (4%) or PS or PG (12%) were immobilized on an L1 sensor chip and pSYT1 32-57 peptides (black bars) and mutant (pSYT1 32-57 $K_{43}A$, $F_{46}A$, $K_{52}A$, gray bars) injected for 1 min at 8 μM. Representative of 2 independent experiments performed in triplicate. Error bars are SD from triplicates. (*F*) Specificity of SYT2 interaction with GT1b inserted in bilayer vesicles. DMPC liposomes containing GT1b (4%) or PS or PG (12%) were immobilized on a L1 sensor chip and pSYT2 40-66 peptides (black bar) and mutants (pSYT2 40-66 $F_{54}A$, $F_{55}A$, gray bar) injected for 1 min at 8 μM. Representative of 2 independent experiments performed in triplicate. Error bars are SD from triplicates.

Fig. S3 *A* and *B*). Addition of GT1b to the longer SYT2 peptide (40-66) used in SPR also induced the formation of an α-helix (*SI Appendix*, Fig. S3*C*). We consequently determined the relative concentration of ganglioside required to induce structural transitions in SYT2. The α-helical transition appeared at a molar ratio of 1:0.5 (peptide:GT1b), reaching a maximum at a molar ratio of 1:3 (*SI Appendix*, Fig. S3*D*). Altogether these results indicate that the extracellular juxtamembrane domain of SYT1 and 2 effectively binds GT1b and that binding induces a transition from a random to an α-helical structure.

Modeling of the SYT/GT1b Interaction. To further assess structural features of the SYT–GT1b complex, we docked GT1b with SYT1 41-71 and SYT2 45-80 amino acid sequences encompassing in continuum their juxtamembrane and TM domains (Fig. 4). In water, these peptides did not fold into a well-defined structure and appeared mostly disordered. When mixed with a model membrane containing ceramide, the TM region of the peptide formed an α-helix. When ceramide was replaced by GT1b, the extracellular part of the peptide adopted an α-helical structure that was clearly induced by the carbohydrate part of GT1b (Fig. 4).

At this stage, the complex displayed a highly complementary structure with a free binding energy of −167.3 and −168 kJ/mol for SYT1 and SYT2, respectively. About two-thirds of this energy (−115.3 and −114) kJ/mol for SYT1 and SYT2, respectively, corresponds to extramembranous interactions (*SI Appendix*, Fig. S4*B*), whereas the remaining third was due to a remarkable fit between the ceramide part of the ganglioside and the TM region of SYT peptides (Fig. 4). The sphingosine and fatty acid chains of the ceramide moiety of GT1b are highly twisted so that they wrap around the TM domain of SYT (Fig. 4). This configuration explains why the membrane-embedded region of the complex has such a high impact (−52/54 kJ/mol) on the energy of interaction of the complex. The complex is stabilized by a combination of van der Waals forces and hydrogen bonds between the polar parts of GT1b and SYT1/2, and by van der Waals forces linking the ceramide part of GT1b and the TM domain of SYT1/2 (*SI Appendix*, Fig. S4 and Table S2). In addition, W_{58} and W_{66} of SYT1 and 2 located at the bilayer interface strongly interacts with both the glycone and ceramide moieties of GT1b (*SI Appendix*, Fig. S4*A*). The minimal distances between SYT1/2 residues and GT1b, including hydrogen atoms, were in the 2- to 3-Å range (*SI Appendix*, Table S2), consistent with the high energy of interaction of each complex (*SI Appendix*, Fig. S4*B*).

Involvement of the Ceramide Domain of GT1b in the SYT/GT1b Interaction. Prompted by the modeling data we probed for a direct interaction between SYT and GT1b in a *cis* configuration (i.e., in the same membrane). For this purpose, the C-terminal part of the extracellular domain of SYT2 was fused to an acyl group to allow membrane insertion (peptidoliposomes; *SI Appendix*, Fig. S5*A*). The acyl group was either a myristyl (Myr) or a farnesyl group (Far). The rationale was that a Myr group will mimic the TM domain of SYT, allowing hydrophobic interaction with the ceramide of GT1b, whereas the Far group will not, due to lateral methyl groups that should interfere with the docking to the ceramide part of GT1b (26). Molecular modeling (*SI Appendix*, Fig. S5 *C*, *Left* and *Middle*) confirmed the similarity of the docking between GT1b and both TM-SYT2 and Myr-SYT2. In contrast and as expected, when the Myr was replaced by a Far moiety (*SI Appendix*, Fig. S5 *C*, *Right*) the latter docked to the opposite face of the GT1b ceramide than Myr and the exposed ceramide face was different.

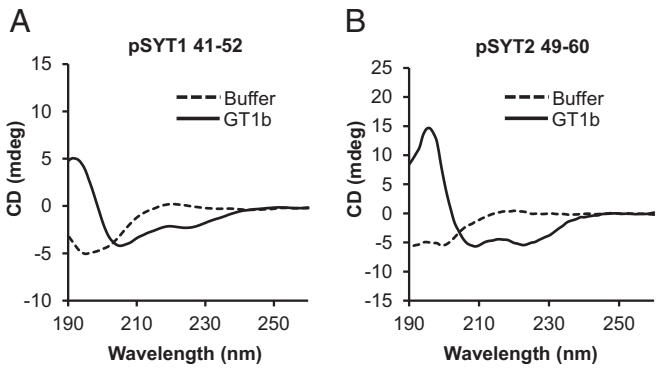

Fig. 3. GT1b induces conformational changes in SYT peptides in solution. Far-ultraviolet CD spectra of the SYT1 (*A*) and 2 (*B*) juxtamembrane extracellular peptides in the absence (dashed lines) or presence (solid line) of GT1b. CD spectra were collected after a 10-min incubation with a molar ratio of 3:1 (ganglioside:peptide). Each spectrum is representative of 2 or 3 experiments and corresponds to the mean of a triplicate determination.

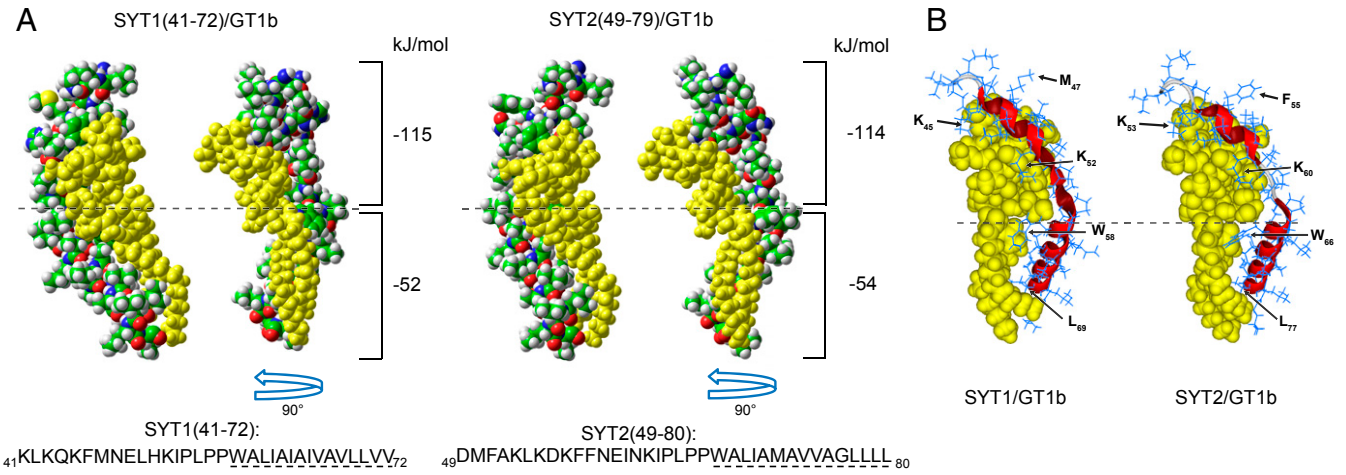

Fig. 4. Molecular modeling of GT1b complexed with SYT1 and SYT2. (*A* and *B*) Molecular models of GT1b complexed with SYT1 (41-72) and SYT2 (49-80) in sphere (*A*) or in sphere/ribbon (*B*) representations. Dashed lines separate the membrane and extramembrane domains. The energy of interaction of each complex is indicated in *A*. Critical amino acid residues involved in each complex are indicated in *B*. Note the kink induced by GT1b in SYT1 and SYT2 (*B*). In all cases, GT1b is colored in yellow. In *A*, the atoms are colored in blue (nitrogen), red (oxygen), green (carbon), and white (hydrogen).

We used spectroscopy to monitor the intrinsic fluorescence of a single tryptophan (W_{66}) residue, located at the lipid–water interface and remarkably sensitive to the polarity of the environment. Soluble SYT2 peptide has maximum peak intensity at 351 nm (*SI Appendix*, Fig. S5*B*, dashed line). Upon insertion of Myr or Far pSYT2 in liposomes the maximum emission peak shifted to 339 nm, indicating that W_{66} is partially buried in a hydrophobic environment at the interface of the lipid bilayer (*SI Appendix*, Fig. S5*B*, solid line and Fig. 5 *A* and *B*, black line) and that the nature of the hydrophobic tail of SYT2 has no influence on the positioning of SYT2 W_{66} relative to the membrane.

Whereas addition of lysolactosylceramide to Myr-pSYT2 peptidoliposome had no effect on the spectra (Fig. 5*A*, green dotted line), GT1b induced a decrease in fluorescence (24 ± 4%, n = 4 independent experiments; Fig. 5*A*, red line). This quenching of tryptophan fluorescence induced by GT1b is compatible

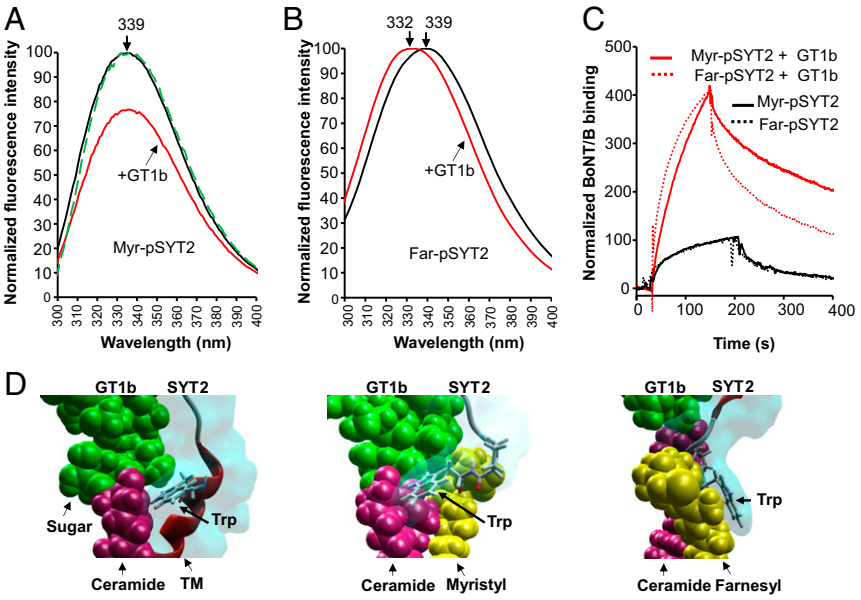

Fig. 5. Involvement of the ceramide domain of GT1b in SYT2/GT1b interaction. (*A* and *B*) Effect of GT1b on SYT2 W_{66} fluorescence. Fluorescence spectra of Myr and Far SYT2 peptides incorporated in liposomes in the absence (black line) or presence (red line) of GT1b at a molar ratio of 3 GT1b:1 peptide. Traces are means of 3 or 4 independent experiments performed in triplicate. Spectrum of Myr-pSYT2 peptide in liposomes in the presence of lyso-lactosyl ceramide is illustrated in *A* (green dotted line). Data were normalized to the relative maximum intensity at the peak wavelength. (*C*) BoNT/B binding to Myr-pSYT2 and Far-pSYT2 peptidoliposomes. Peptidoliposomes and liposomes were immobilized on neutravidin chips and BoNT/B was injected for 2 to 3 min at 30 nM with (upper traces, red) or without (lower traces, black) preaddition of exogenous GT1b. Data were normalized to the maximum response of BoNT/B binding to peptidoliposomes in the absence of GT1b. Representative of 3 independent experiments performed in duplicate. k_{off} values were measured in the presence of GT1b and statistics made using nonparametric Mann–Whitney U test $P = 0.033$. (*D*) Position of tryptophan 66 determined by molecular modeling of the interaction of SYT2 with TM-SYT2, Myr-SYT2, and Far-SYT2 with GT1b. When GT1b is complexed with the natural TM domain of SYT2 or with Myr-SYT2, W_{66} is slightly tilted with respect to the main axis of the ceramide part of GT1b. In this configuration, the indole group remains at the membrane surface with very little insertion. In contrast, in the case of Far-SYT2, W_{66} is vertically oriented and significantly dipped in the membrane.

with the direct interaction scheme presented earlier and especially the molecular modeling data showing that the W_{66} of Myr-pSYT2 interacts with the beta-linked glucose ceramide bond of GT1b and the sia 7 (*SI Appendix*, Fig. S4*A*). The decrease in fluorescence intensity observed with GT1b could be due to GT1b binding inducing α-helix formation in SYT2. The helix would reduce the distance between W_{66} and a charged amino acid such as K_{60}, decreasing electron transfer and thus the emission energy of tryptophan (27, 28).

Addition of GT1b to Far-pSYT2 peptidoliposomes did not modify the peak intensity (3.3% of variation, $n = 3$ independent experiments) but induced a blue shift from 339 ± 1.7 nm to 332 ± 1 nm ($n = 3$ independent experiments), indicating a more hydrophobic environment and suggesting that the tryptophan residue penetrates into the lipid bilayer (Fig. 5*B*, red trace). This result is consistent with molecular modeling in the presence of GT1b, where in Myr-pSYT2 the indole cycle of W_{66} adopts a position parallel to the membrane plane, while in Far-pSYT2 the same indole cycle is perpendicular to the membrane plane and is positioned below the membrane surface (Fig. 5*D*). These results suggest that the interaction of the SYT membrane anchor with the ceramide part of GT1b is involved in the orientation of the extracellular domain of SYT2.

In light of these findings, BoNT/B binding experiments were carried out by SPR using Myr and Far-pSYT2 incorporated in liposomes. In the absence of gangliosides, we observed similar BoNT/B binding kinetics to both types of peptidoliposomes, confirming that the accessibility of the SYT2 peptide to BoNT/B is not modified by the nature of the acyl anchor (Fig. 5*C*, black traces). The addition of GT1b potentiated BoNT/B binding to both types of peptidoliposomes (Fig. 5*C*, red traces) and confirmed that the reconstitution system used allows investigation of the GT1b potentiation of BoNT/B binding. Interestingly, however, the association and dissociation kinetics of BoNT/B binding to Far-pSYT2 relative to Myr-pSYT2 liposomes were modified, notably with a significant 2.5-fold higher dissociation rate ($k_{off} = 7.4 \times 10^{-3} \pm 1.4\ s^{-1}$ and $2.9 \times 10^{-3} \pm 0.6\ s^{-1}$; results are mean ± SEM) from Far-pSYT2 relative to Myr-pSYT2 liposomes, respectively. Altogether, these results indicate that *cis* interactions can occur between SYT2 peptide and GT1b in the same membrane plane and that intramembrane interactions between the ceramide group and the membrane anchor of SYT2 contribute to a precise positioning of the extracellular SYT2–GT1b complex favoring BoNT/B interaction.

Assembly of a SYT–GT1b Complex Plays a Crucial Role in BoNT/B Binding. To pursue the necessity for preassembly of a SYT–GT1b complex to constitute the BoNT/B receptor, we sought to identify a mutation that perturbs SYT binding to GT1b, without inhibiting SYT binding to BoNT/B in the absence of GT1b. We focused on SYT1, which has a stronger GT1b requirement for BoNT/B binding. We therefore mutated K_{52} in SYT1, a highly conserved amino acid predicted to interact with GT1b (Fig. 4*B* and *SI Appendix*, Fig. S4*A*) but not with BoNT/B (9, 16, 18, 19, 29). SPR analysis showed that the K_{52}A mutation in pSYT1 32-57 drastically decreased by 63 ± 13% ($n = 6$ independent experiments) (Fig. 6*A*) its interaction with GT1b, whereas a mutation in another lysine residue (K_{43}) has no significant effect. A control peptide corresponding to the juxtamembrane extracellular domain of SYT9 (pSYT9 27-53), that does not contain a consensus ganglioside-binding motif, accordingly did not show any interaction.

In order to address the effect of K_{52}A on BoNT/B binding in the absence of GT1b, we immobilized both WT and mutant pSYT1 32-57 on SPR sensor chips (Fig. 6*B*). BoNT/B interaction with WT pSYT1 produced square signals with very fast k_{on} and k_{off}, characteristic of low-affinity interactions. These signals were specific as binding of BoNT/E was not detectable (Fig. 6*B*).

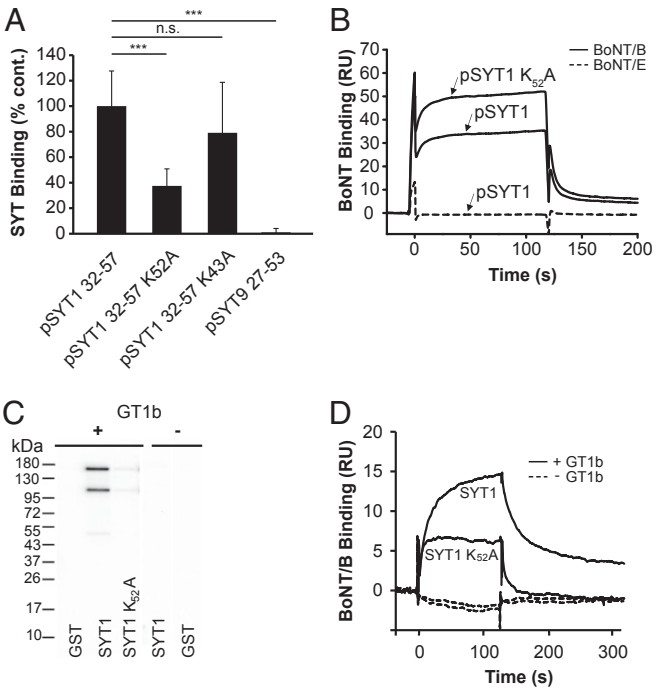

Fig. 6. The juxtamembrane SYT1 lysine residue (K_{52}) is crucial for interaction with GT1b and GT1b potentiation of BoNT/B binding. (*A*) WT or mutant pSYT1 32-57 peptides were injected for 1 min at 8 μM over liposomes containing 4% GT1b and SPR signals recorded at the end of the association phase. Results are mean ± SD of 6 independent experiments. One-way ANOVA followed by Bonferroni's post hoc test was used for statistical analysis (pSYT1 32-57/pSYT1 32-57 K_{43}A $P = 1$ [n.s., nonsignificant]; pSYT1 32-57/pSYT1 32-57 K_{52}A $P = 2.722 \times 10^{-5}$ [***]; pSYT1 32–57/pSYT9 $P = 8.2 \times 10^{-8}$ [***]). (*B*) Effect of SYT1K_{52}A mutation on BoNT/B binding in the absence of GT1b. BoNT/B (30 nM) was injected for 2 min on pSYT peptides (pSYT1 41-52 and pSYT1 41-52 K_{52}A) immobilized on a neutravidin chip and the binding signal recorded at the end of the association phase. BoNT/E (50 nM) binding (dashed curve) to pSYT1 was not distinguishable from the baseline. Data are representative of 3 independent experiments. (*C*) Pull-down assays were carried out with recombinant GST-SYT1 and the K_{52}A mutant immobilized on glutathione-Sepharose beads and incubated with 10 nM BoNT/B in presence or absence of GT1b. Analysis of pellets by protein staining confirmed identical amounts of GST-bait proteins. Pellets were analyzed by immunoblotting to reveal BoNT/B (150 kDa) that was partially reduced (heavy chain 100 kDa). The mutation decreased binding by 88 ± 2% (mean ± SD, $n = 4$). Results are representative of 3 independent experiments. (*D*) BoNT/B binding to full-length WT and K_{52}A mutant GST-SYT1 inserted in liposomes containing GT1b. Proteoliposomes were captured on neutravidin sensor chips and BoNT/B (30 nM) was injected during 2 min. Results are representative of 4 independent experiments. SYT1 K_{52}A mutation induces a 93 ± 10% loss of BoNT/B binding taken at 60 s after the end of injection ($n = 4$ independent experiments; $P = 0.01016$, 1-tailed Mann–Whitney U test). Lower dashed traces show no binding of BoNT/B to either SYT proteoliposomes in the absence of GT1b.

Although GT1b interaction was significantly inhibited by the K_{52}A mutation, (Fig. 6*A*), surprisingly BoNT/B binding to pSYT1 32-57 K_{52}A in the absence of GT1b was enhanced (50 ± 3%, $n = 3$ independent experiments) (Fig. 6*B*). This effect could be explained by the mutation annulling electrostatic repulsion between the positive dipole found in the C-terminus binding domain of BoNT/B (30) and the positive charge of K_{52}.

We then evaluated the effects of the K_{52}A mutation in the full-length protein by pull-down experiments using recombinant GST-SYT1 in detergent. As expected, BoNT/B binding to WT SYT1 was only observed in the presence of GT1b (Fig. 6*C*) (31), whereas the interaction was practically eliminated by the K_{52}A mutation.

We then investigated by SPR the binding of BoNT/B to full-length WT and mutated GST-SYT1 $K_{52}A$ reconstituted in proteoliposomes and immobilized on SPR sensor chips, in the presence of GT1b. Although BoNT/B binding to mutant pSYT1 32-57 $K_{52}A$ was significantly enhanced in the absence of GT1b (Fig. 6*B*), the $K_{52}A$ mutation induced a strong decrease in BoNT/B interaction with a membrane-inserted full-length protein in the presence of GT1b. No binding of BoNT/B was observed in the absence of GT1b (Fig. 6*D*, lower traces). These data clearly show that when preassembly of a SYT–GT1b complex is perturbed subsequent BoNT/B binding is strongly reduced. They are consistent with the proposal that the SYT–GT1b complex constitutes the BoNT/B receptor.

To further investigate whether BoNT/B binding requires preassembly of a GT1b–SYT complex in a cellular context, we investigated the effects of the SYT1 $K_{52}A$ mutation in PC12 cells. PC12 cells were transfected with SYT1 or SYT1 $K_{52}A$, loaded with GT1b and incubated with BoNT/B. The binding of BoNT/B was virtually abolished in cells expressing SYT1 $K_{52}A$ when compared to control cells expressing SYT1 WT (81.4 ± 4.7% of WT-SYT1 vs. 4.0 ± 2.9% of SYT1 $K_{52}A$-transfected cells were positive for BoNT/B labeling) (Fig. 7 *A*, *B*, and *D*). No BoNT/B binding (0.0 ± 0.0%) was observed on cells transfected with the same carrier plasmid devoid of SYT (Fig. 7 *A* and *D*). In order to exclude the possibility of a potential mistargeting of SYT1 $K_{52}A$ that would hinder BoNT/B binding, we performed orthogonal projections of synaptotagmin labeling in both WT-SYT1 and SYT1 $K_{52}A$-transfected cells. No apparent differences in the subcellular distribution of SYT between WT-SYT1 and SYT1 $K_{52}A$-transfected cells were observed (Fig. 7*C*). These results support the conclusion that preassembly of a SYT–GT1b complex is required for BoNT/B to bind to the cell surface.

Discussion

BoNT/B displays remarkable specificity for peripheral nerve terminals conferred by 2 receptor molecules: the synaptic vesicle protein SYT (1 or 2) and the ganglioside GT1b, which although ubiquitous is particularly enriched in axonal terminals. The C-terminal domain of BoNT/B contains 2 distinct binding pockets for 1) an α-helical segment of SYT and 2) a ganglioside (19). This is consistent with the currently predominant schema for independent interaction with dual receptors, in which BoNT/B initially interacts with GT1b then diffuses in the membrane plane until it meets its protein receptor (20). Binding to SYT would then ensure toxin internalization through receptor-mediated endocytosis (21, 32). In this study we first reinvestigated, in a membrane context, BoNT/B binding to each receptor separately and quantified the increase of affinity due to the presence of GT1b. Binding of BoNT/B to PC12 cells expressing or not expressing SYT was addressed in the presence or absence of the glucosyl-ceramide synthase inhibitor PPMP in order to drastically decrease ganglioside level in these cells (31). Careful

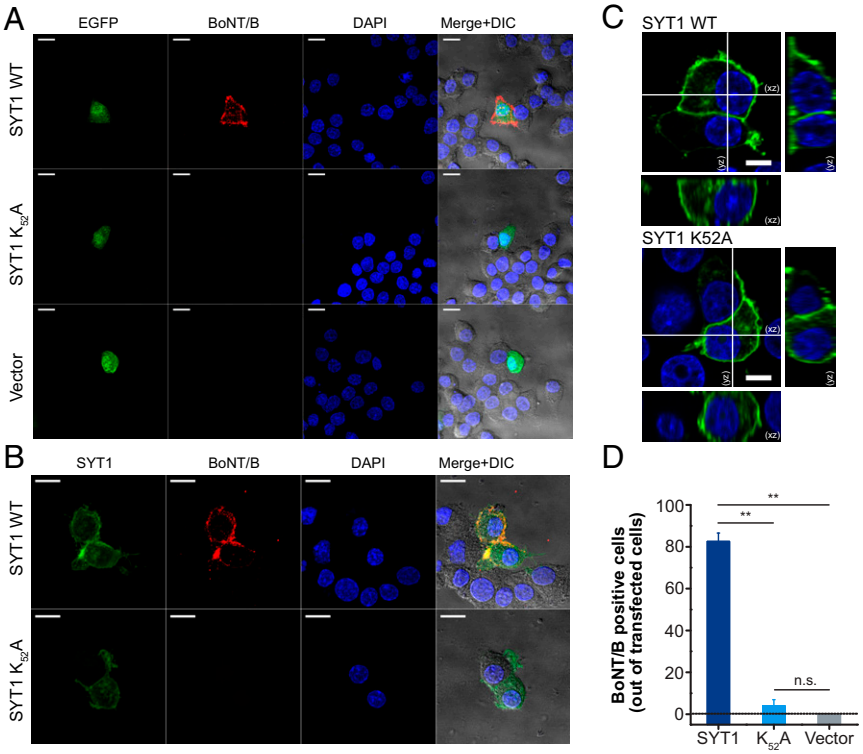

Fig. 7. Mutation of the SYT1 juxtamembrane lysine ($K_{52}A$) inhibits GT1b-dependent BoNT/B binding at the surface of PC12 cells. (*A*) Immunostaining of EGFP (green) and BoNT/B (red) in PC12ΔSYT1 cells expressing full-length WT synaptotagmin 1 (SYT1 WT; *Top*), $K_{52}A$ synaptotagmin 1 (SYT1 $K_{52}A$; *Middle*),, or the EGFP vector alone (*Bottom*). Transfected cells were incubated with 10 nM BoNT/B for 45 min, washed, and fixed as described in *Experimental Procedures*. DAPI signal (blue) was used to reliably quantify the number of cells. Merge over DIC images is shown at the right. (Scale bars, 10 μm.) (*B*) Immunostaining of synaptotagmin 1 (green) and BoNT/B (red) in cells expressing SYT1 WT (*Top*) or SYT1 $K_{52}A$ (*Bottom*). (Scale bars, 10 μm.) (*C*) Orthogonal projections of synaptotagmin 1 labeling in cells transfected with WT synaptotagmin 1 (*Top*) or $K_{52}A$ synaptotagmin 1 (*Bottom*). (Scale bars, 5 μm.) (*D*) Quantification of BoNT/B binding cells in each condition. One-way ANOVA followed by Bonferroni's post hoc test was used for comparisons. Data are expressed as mean ± SEM ($n = 74/93$ cells positive for BoNT/B binding in SYT1 WT transfected cells; $n = 3/100$ cells positive for BoNT/B binding in SYT1 $K_{52}A$ transfected cells; $n = 0/91$ cells positive for BoNT/B binding in control EGFP vector transfected cells). $^{**}P < 0.01$; n.s., nonsignificant; SYT1 WT to SYT1$K_{52}A$ $P = 3.12 \times 10^{-25}$; SYT1 WT to control EGFP vector $P = 3.26 \times 10^{-25}$; SYT1$K_{52}A$ to control EGFP vector $P = 1$.

analysis of binding to PC12 cells and membrane vesicles failed to detect an interaction of BoNT/B with GT1b alone. These findings corroborate previous studies on membrane vesicles or cultured cells not expressing SYT (31, 33–35). Thus, BoNT/B may bind to GT1b with very low affinity (less than micromolar) and rapid dissociation kinetics (22) that rule out detection in assays requiring washing procedures. The absence of BoNT/B binding detection to membrane-associated GT1b may be due to the fact that it has a single ganglioside-binding pocket, in contrast to tetanus toxin, which has 2 and which displays nanomolar affinity for GT1b (36, 37).

In contrast, we readily detected BoNT/B binding to SYT2 expressed in PC12 cells depleted of GT1b, whereas in similar conditions BoNT/B binding to PC12 cells expressing SYT1 cannot be detected in the absence of added gangliosides (31). We then used exosomes expressing recombinant SYT2 to quantify the potentiation by GT1b of BoNT/B binding, in terms of K_d and kinetic constants. This method has revealed an affinity for BoNT/B and association/dissociation rate constants, very close to those found in native membranes (23, 38). SPR measurements in exosomes expressing SYT2 indicated a $K_d = 40$ nM in the absence of GT1b. The addition of exogenous GT1b led to an 80-fold increase in affinity. The large increase in the association rate conferred by GT1b was shown to be dependent on electrostatic interactions as it was totally abolished by an increase in ionic strength of the medium. Gangliosides in neuronal cell membranes contribute strongly to the negative surface charge as they contribute about 75% of plasma membrane sialic acids (39). Moreover, it has been shown that long-range electrostatic interactions between noncontacting residues of the binding partners can play a critical role in the formation of high-affinity complexes (40, 41). Thus, as suggested earlier, gangliosides in anionic microdomains could have a major role in increasing BoNT/B affinity for neuronal membranes through electrostatic interactions involving a positive pole found in the BoNT/B C-terminal domain (30).

BoNT/B has been estimated to have at least 100-fold higher affinity for SYT2 versus SYT1 (16, 29), whereas the addition of GT1b reduces this difference 10-fold (42). Since GT1b enhances BoNT/B affinity for SYT2 by a factor of 80, by extrapolation GT1b would increase the affinity of BoNT/B for SYT1 by a factor of 800. However, it was not possible to quantify the increase in BoNT/B affinity conferred by GT1b to SYT1 as binding of the toxin to SYT1 in a membrane context and in the absence of gangliosides is not detectable (31). The fact that the potentiation by GT1b is more pronounced for SYT1 is particularly important, as SYT1 appears to be the principal BoNT/B receptor in humans (17).

The fact that we were unable to detect BoNT/B binding to GT1b alone, and that GT1b appears to act principally by potentiating binding to SYT, along with SPR data showing that BoNT/B interaction with SYT and GT1b can be fitted with a 1:1 ligand: receptor model, led us to consider the possibility that BoNT/B binds simultaneously, rather than sequentially, to both GT1b and SYT. GT1b-dependent binding to SYT occurred in conditions that severely restrict lateral diffusion, suggesting that a pool of SYT is in sufficient proximity to GT1b to allow BoNT/B to simultaneously bind to both coreceptors. This conclusion is in agreement with independent observations showing that BoNT/B but also BoNT/A are found associated with their corresponding receptors in glycolipid-rich microdomains (43–45).

We then identified a consensus site for ganglioside binding located in extracellular juxtamembrane domains of SYT 1 and 2 and confirmed that peptides covering this region interact directly with GT1b. The site did not display specificity for any particular ganglioside, recognizing other major species in the nerve terminal such as GM1, although the strongest interaction was with GT1b. Interestingly, full-length SYT1 expressed in insect cells has been reported to bind GM1 and GD3 in lipid overlay assays, although the binding domain was not identified (46). We did not detect any interaction with acidic phospholipids, ruling out a simple electrostatic interaction between ganglioside sialic acid and basic residues of the used peptides. The affinity of SYT peptides for the oligosaccharide moiety of GT1b was about $K_d = 3$ μM, comparable to that of saposin for GM1 (47). However, binding parameters measured in a *trans* configuration using a soluble peptide do not take into account additional hydrophobic interactions within the membrane phase.

CD analysis indicated that whereas peptides were unstructured in solution, GT1b induced an increase in α-helical content in both SYT1 and 2. These data were consistent with modeling which showed considerable structural complementarity between GT1b and the juxtamembrane region of SYT1 or 2. The ganglioside can wrap itself around the TM of SYT and interact with the extracellular juxtamembrane domain of SYT that forms an α-helix.

The potentiating effect of GT1b on BoNT/B binding to SYT has only been observed when the 2 receptor components were in the same membrane plane, be it a micelle, liposome, or native membrane (31, 34). Experiments monitoring the fluorescence of an intrinsic tryptophan residue located at the membrane solvent interface confirmed a *cis* interaction between GT1b and SYT2 in a membrane context. Our data indicated that the nature of the acyl group anchoring SYT in the membrane modified the environment of the tryptophan when GT1b was present, consistent with hydrophobic interactions between the peptide membrane anchor and the ceramide moiety. Furthermore, substitution of Myr by Far, precluding appropriate intramembrane interactions with ceramide (24, 48), influenced BoNT/B binding, notably by accelerating dissociation kinetics. These data, associated with modeling, suggest that interactions between the membrane anchors of GT1b and SYT contribute to assembly of the high-affinity BoNT/B receptor site. The association of SYT TM and ceramide confirms initial studies suggesting a SYT/GT1b interaction through hydrophobic domains (34).

The involvement of the hydrophobic domains of SYT and GT1b regarding BoNT/B binding is highlighted by the following observations: 1) SYT1 binds BoNT/B in presence of GT1b only when the TM domain is present and 2) the sugar domain of the ganglioside is not sufficient to potentiate BoNT/B binding to SYT1 or SYT2 (16, 19, 31). Altogether these results suggest that the interaction of SYT and GT1b through intramembrane and extracellular domains is required for BoNT/B binding.

Next we addressed the importance of preassembly of a GT1b–SYT1 complex for BoNT/B binding. The K_{52} residue is located outside of the reported SYT binding pocket of BoNT/B (18) but within the consensus sequence for ganglioside binding and interacts with GT1b in modeling studies. In fact, we demonstrated that the K_{52}A mutation blocks GT1b potentiation of BoNT/B binding to full-length SYT1, in vitro or expressed at the surface of intact PC12 cells. This parallels insulin receptors, which bind GM3 ganglioside upon export to the plasma membrane. In this case the first extracellular lysine following the TM domain is also crucial for ganglioside binding (49).

Structural data show that the short amphipathic helical region, adjacent to the TM domain of SYT1 and SYT2, interacts with BoNT/B in a similar manner (18). The strong dependency on GT1b for BoNT/B binding to SYT1 is thought to be due to the nature of the amino acids (L_{50} and H_{51}) located next to K_{52}, as substitution by the corresponding amino acids of SYT2 rescued BoNT/B binding in the absence of GT1b (9). Our data, showing that K_{52} plays a crucial role in GT1b binding to SYT1, suggest that the interaction of SYT1 with GT1b reduces the inhibitory effects of these vicinal amino acids and induces the formation of an α-helix. Interestingly, a similar phenomenon of α-helix structure induced by the headgroup of gangliosides has been reported for α-synuclein (50) and Alzheimer beta amyloid peptide (51, 52).

Our data suggest that ganglioside could also modulate the secondary structure of a transmembrane protein. In this case, the amphipathic helix would provide structural complementarity between the SYT1 juxtamembrane domain and the SYT binding pocket of BoNT/B, involving mostly hydrophobic residues and complementary salt bridges (18, 19).

We thus propose that upon exocytosis of SYT the SYT–GT1b complex would rapidly assemble, given the large molar ganglioside:SYT ratio at the plasma membrane. BoNT/B would then bind to the N-terminal part of SYT exposed to the extracellular medium and bound to GT1b (Fig. 8). Alternatively, BoNT/B could bind to a resident plasma membrane pool of SYT (53–55) preassembled with GT1b. Interestingly, in view of the fact that SYT can also bind GM1, a similar model could be applied to BoNT/DC, a botulinum subtype toxin that uses GM1 as a coreceptor with SYT (56). The simultaneous binding of BoNT/B to a preassembled coreceptor could thus explain the high affinity and specific binding to the external surface of the presynaptic membrane.

The current results suggest that GT1b may play a triple role in BoNT/B binding: 1) as an electrostatic attractor, 2) in the SYT–GT1b receptor complex, forming and presenting an α-helical segment to the SYT binding pocket, and 3) in stabilizing the toxin receptor complex via the ganglioside binding pocket. Further studies will be necessary to ascertain what happens when the toxin meets the assembled SYT–GT1b complex as certain amino acids crucial for SYT binding to BoNT/B are also involved in the SYT–GT1b interaction. Complementary studies are required to determine whether the toxin could displace the GT1b bound to SYT and if so whether the hydrophobic loop of BoNT/B positioned between the SYT and the GT1b binding pockets is involved.

Experimental Procedures

Reagents. All used reagents are listed in *SI Appendix, SI Experimental Procedures*.

Cloning. Rat SYT 1 and 2 coding sequences were amplified by PCR from a commercial Y2H adult rat brain cDNA library (Origine) and inserted in the bicistronic vector encoding PIRES-EGFP (Clontech). SYT 2 was inserted in nonmodified PIRES-EGFP and a myc tag was included in the reverse primer to generate a C-terminally tagged SYT2. SYT1 was inserted between EcoR1 and Sal1 sites in modified PIRES2-EGFP in which a myc tag was inserted at the beginning of the multiple cloning site between Xho1 and EcoR1. Directed mutagenesis was then used to introduce the $K_{52}A$ mutation in SYT1 and SYT2, respectively. For GST constructs, SYT1 coding sequences were inserted between EcoR1 and Sal1 sites of pGEX4T (GE Healthcare).

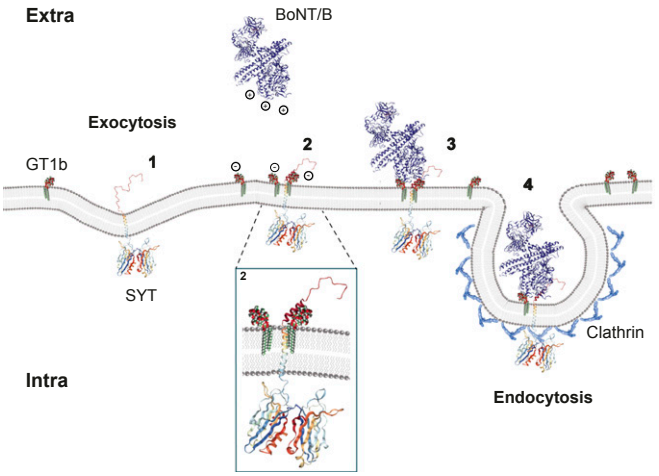

Fig. 8. Schematic model for BoNT/B binding to neuronal membranes. (1) Upon exocytosis, the N-terminal domain of SYT 1 or 2 becomes accessible to the extracellular milieu. (2) It associates with GT1b that is enriched in the external plasma membrane leaflet, inducing formation of an α-helix in the juxtamembrane part of SYT (see zoom in *Inset*). (3) The positive dipole of BoNT/B attracted by negative charges of GT1b interacts simultaneously with GT1b and the SYT–GT1b complex. (4) BoNT/B binding may trigger dissociation of GT1b from SYT by an induced fit mechanism. The cartoon uses adaptations of the following images: BoNT/B image was adapted from Protein Data Bank (PDB) ID code 1F31; SYT1 C2A from PDB ID code 5VFE, C2B from PDB ID code 5VFF, SYT1 TM from PDB ID code 2L8S, and clathrin from PDB ID code 3LVH. The position of binding pockets is schematic.

Recombinant Protein Expression. GST-SYT1 was expressed in BL21 *Escherichia coli* following classical procedures and purified on Glutathione Sepharose in 20 mM Tris·HCl, pH 7.4, 140 mM NaCl, and 0.1% Triton X-100 buffer.

Exosomes. Exosomes expressing SYT2 and AMA1 were produced and purified as described earlier (23) and kept frozen before use.

Liposomal Preparations. Liposomes for SPR lipid-binding specificity experiments: Liposomes were prepared using mixtures of DMPC (1,2-dimyristoyl-*sn*-glycero-3-phosphocholine) with 4% GT1b, 12% PS or 12% PG or 100% of DMPC for control liposomes (850 nmol). Solvent was evaporated and lipids rehydrated in TBS (25 mM Tris·HCl, pH 7.4, and 150 mM NaCl). Liposomes were prepared by extrusion at 55 °C through 100-nm polycarbonate filters using a basic Lipofast apparatus (Avestin). For peptidoliposomes and proteoliposomes see *SI Appendix, SI Experimental Procedures*.

Langmuir Balance. SYT peptide binding to gangliosides was determined using the Langmuir-film balance technique essentially as previously described using a fully automated microtensiometer (μTrough SX; Kibron Inc.) (57). Briefly, interactions were monitored at 20 ± 1 °C by surface pressure modification of monomolecular films of gangliosides resuspended in chloroform/methanol (1:1 vol/vol) and spread on pure water subphases (800 μL). The initial surface pressure of the monolayers was set between 12 and 15 mN/m and the accuracy of measurement conditions was ±0.25 mN/m. SYT peptides were injected (final concentration of 10 μM) into the aqueous phase underneath the ganglioside monolayer until equilibrium was reached and kinetics of surface pressure changes were followed by real-time measurements. Data were analyzed with the FilmWareX program (version 3.57; Kibron Inc.).

CD. CD spectra were obtained at 20 °C in 1-mm-path-length quartz cuvettes using a JASCO model J-810 spectropolarimeter. Thirty micromolar SYT peptide solutions were prepared in filtered 10 mM phosphate buffer, pH 7.6. Gangliosides were added at a final concentration of 90 μM unless otherwise indicated and samples were incubated 10 min before CD analysis.

CD spectra were obtained between 190 nm and 260 nm at 1-nm intervals. Each CD spectrum shown is the average of 3 scans with a scanning speed of 20 nm/min. The spectra were corrected for contributions from buffer and GT1b as appropriate. Data analysis was carried out using the online Dichroweb platform (58, 59) combined with the CDSSTR algorithm. For all CD spectra, the NRMSD parameter (a normalized SD for each curve fit) was below 0.1.

Fluorescence Spectroscopy. Fluorescence spectra were recorded on a Cary Eclipse fluorescence spectrofluorimeter (Varian) with emission and excitation slit widths of 5 nm. Peptidoliposomes containing Myr-SYT2 or Far-SYT2 were diluted in TBS in a total volume of 0.5 mL and the intrinsic fluorescence of SYT2 was recorded in the absence or presence of GT1b or lyso-lactosyl ceramide (23 μM) that were added exogenously with a ganglioside/peptide ratio (mole/mole) of 3. Excitation wavelength was 278 nm. Emission spectra were recorded from 300 to 400 nm, averaging 3 scans. All of the spectra were corrected for the fluorescence of the corresponding blank (liposomes ± GT1b).

Immunofluorescence Staining. PC12 cells deficient in SYT1 and 2 (PC12ΔSYT1) were cultured on poly-L-lysine–treated (10 μg/mL) coverslips (300,000 cells per well) in Dulbecco's modified Eagle's medium (DMEM) containing 5% fetal bovine serum, 5% horse serum, and 1% penicillin/streptomycin mixture. Where stated, 7.5 μM of the "glucosyl-ceramide synthase" inhibitor PPMP was added to the culture medium for 48 h. Cells were transfected with the corresponding plasmids (pIRES-EGFP, pIRES-EGFP-SYT1, or pIRES-EGFP-SYT2) using Lipofectamine 2000 and following the manufacturer's procedure. Forty hours after transfection and when appropriate GT1b (10 μg/mL) was added to the wells in DMEM and incubated for 1.5 h at 37 °C. BoNT/B at the indicated concentrations or a mixture of BoNT/B and anti-SYT2 antibody (8G2b 1 μg/mL) were then added to the culture medium and incubated for 45 min at 37 °C.

After a first wash with the culture medium, additional washes were performed with phosphate-buffered saline (PBS) and cells were fixed in the dark at 4 °C in 4% paraformaldehyde/PBS followed by NH_4Cl washing steps. Nonspecific binding was blocked with 0.2% (wt/vol) gelatin or 5% (vol/vol) goat serum in a PBS buffer containing 0.1% saponin. Anti-BoNT/B (0.5 μg/μL), anti-GFP (2 μg/mL), 1D12 anti-SYT (1 μg/mL), or anti-GT1b (1:1,000) antibodies were then added for 45 min at 22 °C. After subsequent washing, staining was visualized using secondary anti-rabbit Alexa 594 or 555 and anti-mouse Alexa 647-nm or 488-nm antibodies. Nuclei were detected using DAPI.

Confocal Microscopy and Quantitative Analyses. Confocal images were acquired on a Zeiss LSM780 microscope and analyzed using ImageJ (https://imagej.nih.gov/ij/). PPMP effects were presented as ratios of relative intensities to mean fluorescence values obtained in the absence of PPMP. Results are shown as mean ± SD and statistical analysis were done using Mann–Whitney *U* test. Results of BoNT/B binding to nontransfected, WT SYT1 and mutant SYT1-K_{52}A expressing PC12 were presented as means ± SEM and 1-way ANOVA followed by Bonferroni's post hoc test was used for comparisons.

Cellular ELISA. PC12 cells (300,000 per well) were cultured directly on plastic 24-well plates pretreated with poly-L-lysine (10 μg/mL). Cells were transfected with SYT2 or carrier vector and treated when appropriate with PPMP as for immunofluorescence experiments. BoNT/B (5 nM) or a mixture of BoNT/B and the neutralizing anti-BoNT/B antibody (100 nM) were then added to the culture medium and incubated for 1 h on ice. Cells were washed with PBS and fixed at 4 °C in 4% paraformaldehyde/PBS. A 45-min consecutive blocking step with 0.056% saponin and 0.2% gelatin in PBS was preceded by 2 × 5-min NH_4Cl washing steps. Anti-BoNT/B (0.5 μg/μL) was then added for 1 h at 22 °C in the blocking buffer. Three washing steps were performed with the blocking buffer before adding the secondary HRP-coupled anti-rabbit antibody for an additional hour at 22 °C. Cells were washed 5 times with the blocking buffer and the HRP substrate TMB was added. The colorimetric reaction was stopped by H_2SO_4 and the optical density measured at 450 nm.

Molecular Modeling. In silico analyses were performed using Hyperchem and Molegro Molecular viewer as described (60). The initial coordinates of GT1b were obtained from CHARMM-GUI Glycolipid Modeler (http://www.charmm-gui.org/?doc=input/glycolipid; ref. 61), which uses the internal coordinate information of common glycosidic torsion angle values, orients the ganglioside perpendicular to the membrane, and performs Langevin dynamics with a cylindrical restraint potential to keep the whole GT1b molecule cylindrical. In the next step, we included GT1b in a periodic box (30 × 30 × 50 Å) solvated with 1,487 water molecules. The system was energy-minimized 6 times switching alternatively between runs using steepest descent gradients or Polak–Ribière conjugate gradients until convergence to machine precision. GT1b was then merged with energy-minimized SYT1 or SYT2 peptides generated de novo with the amino acid database of Hyperchem. Initial conditions of SYT 1/2 and GT1b (sphingosine/C18:0) corresponded to minimized structures obtained with the Polak–Ribière algorithm. Docked SYT–GT1b complexes were subsequently submitted to iterative cycles of molecular dynamics using the CHARMM36 force field optimized for sphingolipids (62) and carbohydrates (63). Interaction energies were calculated from stable complexes after several 10-ns cycles using the Ligand Energy Inspector function of Molegro.

SPR. SPR measurements were conducted at 25 °C at a flow rate of 30 μL/min on a Biacore 3000 or Biacore T200 (GE Healthcare Life Sciences). For details see *SI Appendix, SI Experimental Procedures*.

Pull-Down Experiments. GST and GST-SYT1 (10 μg) were immobilized on glutathione Sepharose 4B resin. Washed beads were incubated in TBST (25 mM Tris·HCl, pH 7.4, 150 mM NaCl, and 0.1% Triton X-100) with BoNT/B (10 nM) for 1 h at 4 °C, in the presence or absence of GT1b (25 μg/mL). The beads were washed and bound proteins boiled 5 min in SDS-sample buffer containing 10 mM dithiothreitol and analyzed by immunoblot using anti-BoNT/B antibody at 0.5 μg/mL (Metabiologics). Red Ponceau detection was used to ensure that equal amounts of bait protein were captured on the beads.

ACKNOWLEDGMENTS. We thank Nouara Yahi and Raymond Miquelis for helpful discussions and Robert Mamoun (Ciloa SAS) for exosome production. This work was financially supported by INSERM and Aix-Marseille University. PhD fellowships of A.F. and R.D. were co-financed by INSERM and the Region SUD (Provence Alpes Côte d'Azur). Ciloa SAS cofunded the PhD fellowship of R.D. We thank the Agence Nationale de la Recherche for financially supporting J.R.-F.

1. B. Poulain, M. R. Popoff, Why are botulinum neurotoxin-producing bacteria so diverse and botulinum neurotoxins so toxic? *Toxins (Basel)* **11**, E34 (2019).
2. L. Simpson, The life history of a botulinum toxin molecule. *Toxicon* **68**, 40–59 (2013).
3. A. P. Tighe, G. Schiavo, Botulinum neurotoxins: Mechanism of action. *Toxicon* **67**, 87–93 (2013).
4. R. A. Kammerer, R. M. Benoit, Botulinum neurotoxins: New questions arising from structural biology. *Trends Biochem. Sci.* **39**, 517–526 (2014).
5. S. N. Fewou, J. J. Plomp, H. J. Willison, The pre-synaptic motor nerve terminal as a site for antibody-mediated neurotoxicity in autoimmune neuropathies and synaptopathies. *J. Anat.* **224**, 36–44 (2014).
6. S. Salinas, G. Schiavo, E. J. Kremer, A hitchhiker's guide to the nervous system: The complex journey of viruses and toxins. *Nat. Rev. Microbiol.* **8**, 645–655 (2010).
7. J. Fantini, N. Yahi, *Brain Lipids in Synaptic Function and Neurological Disease: Clues to Innovative Therapeutic Strategies for Brain Disorders* (Elsevier, 2015).
8. R. L. Schnaar, Gangliosides of the vertebrate nervous system. *J. Mol. Biol.* **428**, 3325–3336 (2016).
9. Q. Chai *et al.*, Structural basis of cell surface receptor recognition by botulinum neurotoxin B. *Nature* **444**, 1096–1100 (2006).
10. C. Montecucco, O. Rossetto, G. Schiavo, Presynaptic receptor arrays for clostridial neurotoxins. *Trends Microbiol.* **12**, 442–446 (2004).
11. S. Sonnino, M. Aureli, L. Mauri, M. G. Ciampa, A. Prinetti, Membrane lipid domains in the nervous system. *Front. Biosci.* **20**, 280–302 (2015).
12. L. H. Chamberlain, R. D. Burgoyne, G. W. Gould, SNARE proteins are highly enriched in lipid rafts in PC12 cells: Implications for the spatial control of exocytosis. *Proc. Natl. Acad. Sci. U.S.A.* **98**, 5619–5624 (2001).
13. J. Yao, S. E. Kwon, J. D. Gaffaney, F. M. Dunning, E. R. Chapman, Uncoupling the roles of synaptotagmin I during endo- and exocytosis of synaptic vesicles. *Nat. Neurosci.* **15**, 243–249 (2011).
14. S. E. Kwon, E. R. Chapman, Glycosylation is dispensable for sorting of synaptotagmin 1 but is critical for targeting of SV2 and synaptophysin to recycling synaptic vesicles. *J. Biol. Chem.* **287**, 35658–35668 (2012).
15. E. R. Chapman, A Ca^{2+} sensor for exocytosis. *Trends Neurosci.* **41**, 327–330 (2018).
16. R. Jin, A. Rummel, T. Binz, A. T. Brunger, Botulinum neurotoxin B recognizes its protein receptor with high affinity and specificity. *Nature* **444**, 1092–1095 (2006).
17. L. Peng *et al.*, Botulinum neurotoxin D-C uses synaptotagmin I and II as receptors, and human synaptotagmin II is not an effective receptor for type B, D-C and G toxins. *J. Cell Sci.* **125**, 3233–3242 (2012).
18. M. Elliott *et al.*, Engineered botulinum neurotoxin B with improved binding to human receptors has enhanced efficacy in preclinical models. *Sci. Adv.* **5**, eaau7196 (2019).
19. R. P. Berntsson, L. Peng, M. Dong, P. Stenmark, Structure of dual receptor binding to botulinum neurotoxin B. *Nat. Commun.* **4**, 2058 (2013).
20. C. Montecucco, How do tetanus and botulinum toxins bind to neuronal membranes? *Trends Biochem. Sci.* **11**, 314–317 (1986).
21. G. Schiavo, Structural biology: Dangerous liaisons on neurons. *Nature* **444**, 1019–1020 (2006).
22. D. Stern *et al.*, A lipid-binding loop of botulinum neurotoxin serotypes B, DC and G is an essential feature to confer their exquisite potency. *PLoS Pathog.* **14**, e1007048 (2018).
23. R. Desplantes *et al.*, Affinity biosensors using recombinant native membrane proteins displayed on exosomes: Application to botulinum neurotoxin B receptor. *Sci. Rep.* **7**, 1032 (2017).
24. J. Fantini, N. Garmy, N. Yahi, Prediction of glycolipid-binding domains from the amino acid sequence of lipid raft-associated proteins: Application to HpaA, a protein involved in the adhesion of Helicobacter pylori to gastrointestinal cells. *Biochemistry* **45**, 10957–10962 (2006).
25. J. Fantini, N. Yahi, Molecular basis for the glycosphingolipid-binding specificity of α-synuclein: Key role of tyrosine 39 in membrane insertion. *J. Mol. Biol.* **408**, 654–669 (2011).
26. I. Levental, M. Grzybek, K. Simons, Greasing their way: Lipid modifications determine protein association with membrane rafts. *Biochemistry* **49**, 6305–6316 (2010).
27. L. M. Loura, R. F. de Almeida, A. Coutinho, M. Prieto, Interaction of peptides with binary phospholipid membranes: Application of fluorescence methodologies. *Chem. Phys. Lipids* **122**, 77–96 (2003).
28. T. Liu *et al.*, Ionization potentials of fluoroindoles and the origin of nonexponential tryptophan fluorescence decay in proteins. *J. Am. Chem. Soc.* **127**, 4104–4113 (2005).
29. L. Tao *et al.*, Engineered botulinum neurotoxin B with improved efficacy for targeting human receptors. *Nat. Commun.* **8**, 53 (2017).
30. F. Fogolari, S. C. Tosatto, L. Muraro, C. Montecucco, Electric dipole reorientation in the interaction of botulinum neurotoxins with neuronal membranes. *FEBS Lett.* **583**, 2321–2325 (2009).
31. M. Dong *et al.*, Synaptotagmins I and II mediate entry of botulinum neurotoxin B into cells. *J. Cell Biol.* **162**, 1293–1303 (2003).
32. S. Pellett, W. H. Tepp, J. M. Scherf, E. A. Johnson, Botulinum neurotoxins can enter cultured neurons independent of synaptic vesicle recycling. *PLoS One* **10**, e0133737 (2015).

33. M. Dong, W. H. Tepp, H. Liu, E. A. Johnson, E. R. Chapman, Mechanism of botulinum neurotoxin B and G entry into hippocampal neurons. *J. Cell Biol.* **179**, 1511–1522 (2007).
34. S. Kozaki, Y. Kamata, S. Watarai, T. Nishiki, S. Mochida, Ganglioside GT1b as a complementary receptor component for Clostridium botulinum neurotoxins. *Microb. Pathog.* **25**, 91–99 (1998).
35. S. Sun *et al*., Receptor binding enables botulinum neurotoxin B to sense low pH for translocation channel assembly. *Cell Host Microbe* **10**, 237–247 (2011).
36. P. Lazarovici, E. Yavin, Tetanus toxin interaction with human erythrocytes. I. Properties of polysialoganglioside association with the cell surface. *Biochim. Biophys. Acta* **812**, 523–531 (1985).
37. C. Chen, Z. Fu, J. J. Kim, J. T. Barbieri, M. R. Baldwin, Gangliosides as high affinity receptors for tetanus neurotoxin. *J. Biol. Chem.* **284**, 26569–26577 (2009).
38. J. O. Dolly *et al*., Localization of sites for 125I-labelled botulinum neurotoxin at murine neuromuscular junction and its binding to rat brain synaptosomes. *Toxicon* **20**, 141–148 (1982).
39. R. L. Schnaar, R. Gerardy-Schahn, H. Hildebrandt, Sialic acids in the brain: Gangliosides and polysialic acid in nervous system development, stability, disease, and regeneration. *Physiol. Rev.* **94**, 461–518 (2014).
40. B. A. Joughin, D. F. Green, B. Tidor, Action-at-a-distance interactions enhance protein binding affinity. *Protein Sci.* **14**, 1363–1369 (2005).
41. D. M. Lesovoy *et al*., Specific membrane binding of neurotoxin II can facilitate its delivery to acetylcholine receptor. *Biophys. J.* **97**, 2089–2097 (2009).
42. T. Nishiki *et al*., The high-affinity binding of Clostridium botulinum type B neurotoxin to synaptotagmin II associated with gangliosides GT1b/GD1a. *FEBS Lett.* **378**, 253–257 (1996).
43. C. Gil, A. Soler-Jover, J. Blasi, J. Aguilera, Synaptic proteins and SNARE complexes are localized in lipid rafts from rat brain synaptosomes. *Biochem. Biophys. Res. Commun.* **329**, 117–124 (2005).
44. J. Herreros, G. Schiavo, Lipid microdomains are involved in neurospecific binding and internalisation of clostridial neurotoxins. *Int. J. Med. Microbiol.* **291**, 447–453 (2002).
45. L. Muraro, S. Tosatto, L. Motterlini, O. Rossetto, C. Montecucco, The N-terminal half of the receptor domain of botulinum neurotoxin A binds to microdomains of the plasma membrane. *Biochem. Biophys. Res. Commun.* **380**, 76–80 (2009).
46. M. Vrljic *et al*., Post-translational modifications and lipid binding profile of insect cell-expressed full-length mammalian synaptotagmin 1. *Biochemistry* **50**, 9998–10012 (2011).
47. M. J. Champagne, S. Lamontagne, M. Potier, Binding of GM1 ganglioside to a synthetic peptide derived from the lysosomal sphingolipid activator protein saposin B. *FEBS Lett.* **349**, 439–441 (1994).
48. K. A. Melkonian, A. G. Ostermeyer, J. Z. Chen, M. G. Roth, D. A. Brown, Role of lipid modifications in targeting proteins to detergent-resistant membrane rafts. Many raft proteins are acylated, while few are prenylated. *J. Biol. Chem.* **274**, 3910–3917 (1999).
49. K. Kabayama *et al*., Dissociation of the insulin receptor and caveolin-1 complex by ganglioside GM3 in the state of insulin resistance. *Proc. Natl. Acad. Sci. U.S.A.* **104**, 13678–13683 (2007).
50. Z. Martinez, M. Zhu, S. Han, A. L. Fink, GM1 specifically interacts with alpha-synuclein and inhibits fibrillation. *Biochemistry* **46**, 1868–1877 (2007).
51. J. McLaurin, T. Franklin, P. E. Fraser, A. Chakrabartty, Structural transitions associated with the interaction of Alzheimer beta-amyloid peptides with gangliosides. *J. Biol. Chem.* **273**, 4506–4515 (1998).
52. K. Matsuzaki, How do membranes initiate Alzheimer's disease? Formation of toxic amyloid fibrils by the amyloid β-protein on ganglioside clusters. *Acc. Chem. Res.* **47**, 2397–2404 (2014).
53. Y. Hua *et al*., A readily retrievable pool of synaptic vesicles. *Nat. Neurosci.* **14**, 833–839 (2011).
54. T. Fernández-Alfonso, R. Kwan, T. A. Ryan, Synaptic vesicles interchange their membrane proteins with a large surface reservoir during recycling. *Neuron* **51**, 179–186 (2006).
55. K. I. Willig, S. O. Rizzoli, V. Westphal, R. Jahn, S. W. Hell, STED microscopy reveals that synaptotagmin remains clustered after synaptic vesicle exocytosis. *Nature* **440**, 935–939 (2006).
56. S. Zhang *et al*., Structural basis for the unique ganglioside and cell membrane recognition mechanism of botulinum neurotoxin DC. *Nat. Commun.* **8**, 1637 (2017).
57. C. Di Scala, H. Chahinian, N. Yahi, N. Garmy, J. Fantini, Interaction of Alzheimer's β-amyloid peptides with cholesterol: Mechanistic insights into amyloid pore formation. *Biochemistry* **53**, 4489–4502 (2014).
58. L. Whitmore, B. A. Wallace, DICHROWEB, an online server for protein secondary structure analyses from circular dichroism spectroscopic data. *Nucleic Acids Res.* **32**, W668–W673 (2004).
59. A. Lobley, L. Whitmore, B. A. Wallace, DICHROWEB: An interactive website for the analysis of protein secondary structure from circular dichroism spectra. *Bioinformatics* **18**, 211–212 (2002).
60. C. Di Scala, J. Fantini, Hybrid in silico/in vitro approaches for the identification of functional cholesterol-binding domains in membrane proteins. *Methods Mol. Biol.* **1583**, 7–19 (2017).
61. J. Lee *et al*., CHARMM-GUI membrane builder for complex biological membrane simulations with glycolipids and lipoglycans. *J. Chem. Theory Comput.* **15**, 775–786 (2019).
62. R. M. Venable *et al*., CHARMM all-atom additive force field for sphingomyelin: Elucidation of hydrogen bonding and of positive curvature. *Biophys. J.* **107**, 134–145 (2014).
63. O. Guvench *et al*., Additive empirical force field for hexopyranose monosaccharides. *J. Comput. Chem.* **29**, 2543–2564 (2008).